Discrete Element Analysis on Mechanical Properties of Ballast Bed by Tamping in Railway Turnout Areas

Chi, Yihao; Xiao, Hong; Zhang, Zhihai; Fang, Shuwei; Wang, Haoyu

Yihao Chi
School of Civil Engineering,
Beijing Jiaotong University,
Beijing 100044, China;
Beijing Key Laboratory of Track Engineering,
Beijing Jiaotong University,
Beijing 100044, China

Hong Xiao[1]
Professor
School of Civil Engineering,
Beijing Jiaotong University,
Beijing 100044, China;
Beijing Key Laboratory of Track Engineering,
Beijing Jiaotong University,
Beijing 100044, China
e-mail: xiaoh@bjtu.edu.cn

Zhihai Zhang
School of Civil Engineering,
Beijing Jiaotong University,
Beijing 100044, China;
Beijing Key Laboratory of Track Engineering,
Beijing Jiaotong University,
Beijing 100044, China

Shuwei Fang
Beijing Mass Transit Railway Operation
Corporation,
The Line Branch Company,
Beijing 100082, China

Haoyu Wang
Engineering Structures Department,
Delft University of Technology,
Delft 2628, The Netherlands

Discrete Element Analysis on Mechanical Properties of Ballast Bed by Tamping in Railway Turnout Areas

Turnout is the key component of the railway tracks for trains to change direction, which is vital to operational safety and passenger comfort. Therefore, it is of great importance to perform a scientific and reasonable tamping operation for turnout areas. In this paper, based on the commercial software EDEM and RECURDYN, a coupled simulation model of the large machine tamping device-rail-sleeper-ballast bed in the turnout area is jointly established, and the correctness of the model is verified by the test results of the lateral resistance of the ballast bed. The influence of tamping operation on the macro-and micromechanical properties of ballast bed at the switching part of railway turnout areas is studied and recommendations for the optimization of tamping operation are proposed. The results show that in the squeezing stage, strong force chains are distributed concentrately under sleepers, where the distribution range is approximately elliptical with a depth of 150 mm. After tamping, only the 200-mm ballast under the sleepers is compacted, where the compactness is increased by 5.9%. On the contrary, the compactness of the ballast in the sleeper crib is reduced by 27.4%, which is the weakest part. To ensure favorable tamping quality, the tamping sequence at the switching part of railway turnout areas is suggested to be conducted in order of first through track and then diverging track. [DOI: 10.1115/1.4055429]

Keywords: ballast track, turnout, tamping operation, discrete element method (DEM), macro and micro mechanical properties

1 Introduction

Currently in operation, heavy-haul railways and trunk railways mainly adopt ballast track structures in China. The ballast bed is composed of various particle sizes of cohesionless crushed stone, which is an important part of ballast tracks [1]. Under the influence of cyclic loading of trains and the natural environment such as wind, rain, snow, ballast is gradually crushed and powdered, resulting in problems such as line irregularities, which affect the safety of operations [2,3]. The turnout is the key component in railway tracks for trains to change direction, and it is one of the most important infrastructures for operational safety and passenger comfort [4,5]. Due to the structural discontinuity and irregularity of turnouts, the wheel–rail interaction is often intensified when passing through the turnouts. As a result, the impact of trains on the ballast bed is much larger, which makes it easy to loosen the track structure and thus threaten operational safety. In recent years, many train derailments have occurred in turnout areas. For example, two derailments occurred consecutively at the turnout area on the Datong–Qinhuangdao heavy-haul railway derailed in August 2020. A derailment occurred on the Qinghai–Tibet Railway due to excessive wear at the switching part of the turnout area in July 2012. A solution to maintain turnouts is tamping operations using a tamping machine.

Many studies have been carried out on the operation mechanism of tamping machines and the damage they may cause to the ballast bed. Guo et al. [6] systematically summarized the research progress of tamping operation, and proposed many challenges and prospects, which laid a foundation and provided a lot of guiding significance for the future research work. In the aspect of experimental research, Przybyłowicz et al. [7] explored the differences between the vertical tamping method and the lateral tamping method through laboratory experiments, and the results showed that the lateral tamping method was more conducive to improving the compactness of the sleeper end ballast. Kumara and Hayano [8] studied the settlement characteristics of ballast samples in different soiled states after tamping operation with the help of an indoor scale test platform. The results showed that the tamping operation plan of the soiled ballast bed was closely related to the soiling rate. McDowell et al. [9] established an indoor tamping test bench with a ballast bed and the influence of tamping operation on the crushing and wear of ballast particles were analyzed using the Los Angeles Abrasion and Micro-Deval Attrition. Douglas [10] carried out a series of laboratory tests using small tamping equipment to analyze the impact of the tamping operation on the crushing of ballast particles and got recommendations for ballast selection. Aingaran et al. [11] conducted a triaxial test after tamping. The results showed that the tamping operation destroyed the structure and elasticity of the ballast bed and had a destructive effect on the stability of the ballast bed and the ballast particles. Wang et al. [12] conducted field tests on the ballast bed of the Changsha–Zhuzhou–Xiangtan intercity railway in China and

found that the resistance of the ballast bed and the number of tamping were not strictly linear. The ballast bed reached its best condition after the sixth tamping. When the sleeper displacement was about 4 mm, the resistance of the ballast bed tended to be stable.

In the aspect of numerical simulation, Tutumluer et al. [13] used the three-dimensional discrete element analysis software DBLOKS3D to simulate the tamping operation of a tamping machine and compared the change of lateral resistance of ballast bed before and after the tamping operation using the image analysis method. They found that the shape of ballast particles had a bearing on the change in the lateral resistance of the ballast bed. Saussine et al. [14,15] also used the discrete element method (DEM) and found that the tamping operation changed the occlusion and contact state of ballast particles, resulting in a decrease in the overall strength of ballast bed. The research of Wang et al. [16,17] showed that the ballast under sleepers had better stability when the vibrating frequency was 35–45 Hz. Shi et al. [18,19] developed a model consisting of four sleepers. The results showed that the tamping operation had the most significant impact on the ballast in the sleeper cribe and under the sleeper, where the ballast particles were easy to break. Zhou et al. [20] studied the quality evaluation method before and after tamping operation. The discrete element method was used to analyze the change of ballast bed compactness, and the model was verified by experimental results based on water-filling method. Feng [21] analyzed the mechanism of the tamping operation by using the COSMOSMOTION software and the finite element software ANSYS. The results showed that the energy generated by tamping picks was transmitted to the ballast bed in the form of vibration waves, thus making the ballast bed more compact.

In summary, many scholars have researched the tamping operation in ballast track. However, the models in the existing studies are incomplete enough, and they mainly focus on the main line section, while the mechanics of the tamping operation in the turnout areas has been barely studied. In fact, the tamping machine, tamping method, tamping operation parameters, and sleeper size used in the turnout areas are significantly different from those in the main line section, and there are some specific problems such as tamping sequence of four rails, so the tamping operation process is more complicated. Due to the lack of theoretical basis, the tamping operation in the turnout areas mainly relies on the practical experience of the operators at present. Based on this, the paper combines the discrete element software (EDEM) and multibody dynamics software (RECURDYN) to develop a dynamic model to study the tamping operation of the commonly used CDC-16 turnout tamping machine in the turnout areas. The model consists of the tamping device, rail, sleeper, and ballast bed and is used to analyze the distribution of contact force and coordination number at different parts of the ballast bed during the tamping operation. After that, the movement of ballast particles and the change in the compactness of the ballast bed are discussed. Using the model, the effect of the tamping operation and its sequence are studied, hoping to provide scientific guidance for the maintenance and repair operations of the turnout areas.

2 Numerical model

2.1 Model development. The switching part is an important component of the turnout, which undertakes the transition of the wheel loads and steering of trains [22]. There are four rails at the switching part (from the switch point to crossing nose/frog), and the gap between the stock rail and the switching blade is too small for the double-pick insertion. As a result, only the single-pick insertion can be performed and the quality of the tamping operation has not been reported in the literature. Thus, the paper develops a model at the switching part of turnout areas to study the effect of the tamping operation, as shown in Fig. 1.

The single turnout No. 12 is studied, which is commonly used in the Chinese railways. The rail of 60 kg/m is used in the model.

The parameters of the first-level ballast used on existing lines [23] are used, and the gradation of which is shown in Fig. 2.

In the DEM, the continuum is usually simulated as the geometric body, which is regarded as the fixed boundary. As a result, it is difficult to accurately simulate the complex motion of the continuum. On the contrary, the multibody dynamics (MBD) is mainly used for the simulation of the continuum and thus unsuitable for granular materials. Therefore, the paper combines the DEM software and MBD software to study the tamping operation in the turnout. By using the coupling algorithm, the advantages of the two methods can be exerted at the same time so that the tamping process can be accurately simulated and the interaction between the tamping picks, sleepers, and ballast particles can be correctly calculated. The coupling of the two methods is shown in Fig. 3.

Since there is no direct contact between rail and ballast during tamping operation and the force transmission mechanism between rail and sleeper has little effect on tamping operation, the connection between rail and sleeper is simplified as a fixed pair. The specific modeling steps are as follows:

- Ballast particles are modeled by spherical particles and the model of ballast bed is constructed by layering. First, according to section size of ballast bed, ballast particles are put in a cuboid of $5790 \times 2100 \times 350\ \mathrm{mm}^3$, wherein the gradation in Fig. 2 is used.
- The sleepers are modeled in 3D modeling software. After that, they are saved as a "step" file and imported into the DEM software. Three sleepers are placed on the cuboid established in the previous step and the sleeper spacing is 600 mm.
- The top surface of the ballast bed in the turnout section with sleepers should be 3 cm lower than the track bearing surface. Since the height of the sleepers is 220 mm, the buried depth of the sleepers is 190 mm. Moreover, ballast particles are continuously generated using the same gradation to meet the demand.
- Compact the ballast bed shoulders using wall elements to achieve the slope of 1:1.75. In the final ballast bed model, the compactness is 64.5%.
- According to the dimension measured on site, the tamping device is modeled in a 3D modeling software, which is saved as a step file imported into the MBD software together with the rail (60 kg/m) and sleeper models.
- The calculation parameters for the models are set in the MBD software and then they are saved as some "wall" files for information transmission. Import these files into the DEM software to develop a bidirectional-coupled DEM–MBD model of the turnout area, as shown in Fig. 4. The dimensions of the model are shown in Table 1.

In the model established in this paper, there are about 480,000 particles in total, and the calculation is performed on a computer with six cores and 12 threads. The processor is Intel® CoreTMi7-10750H@2.60 GHz, the running memory is 8 GB, and the time-step is set to 5×10^{-6} s. Set the time of one tamping operation to 2.072 s, and the actual calculation time is about 27 h.

2.2 Contact model. Contact is the key to discrete element modeling analysis [24]. The interaction between two ballast particles and between a ballast particle and a geometric body in the model is based on the Hertz–Mindlin contact model, as shown in Fig. 5.

In Fig. 5, R_0 is the contact radius and α_n is the normal overlap, which are the most important parameters for contact identification and movement calculation. R_0 and α_n are expressed as follows:

$$\alpha_n = R_1 + R_2 - |\mathbf{r_1} - \mathbf{r_2}| \tag{1}$$

$$R_0 = \sqrt{\alpha_n R^*} \tag{2}$$

where $\mathbf{r_1}$ and $\mathbf{r_2}$ are the position vectors of two particle centers, and R^* is the equivalent radius.
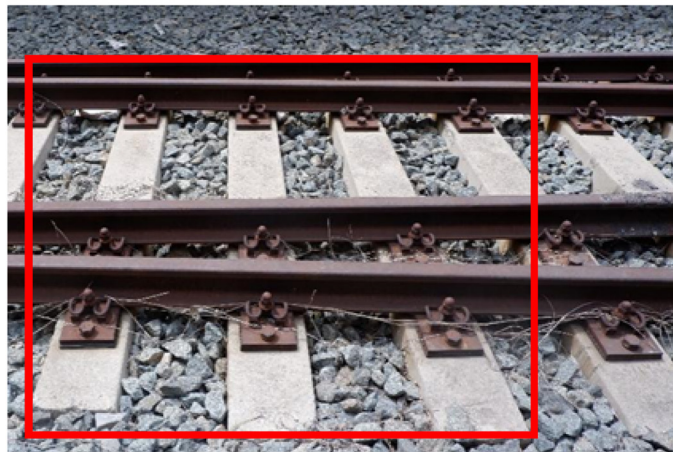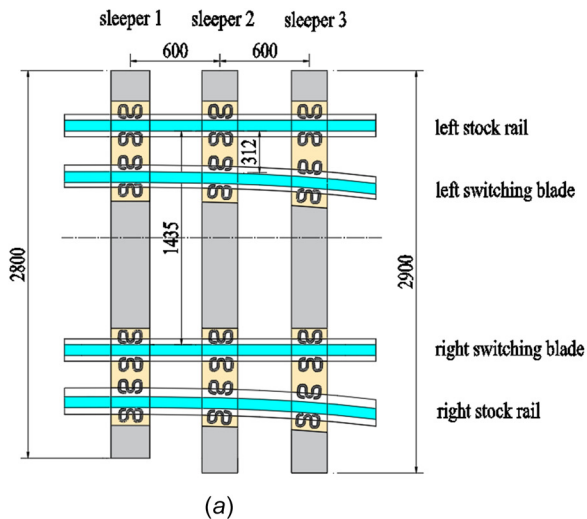
Fig. 1 Modeling area: (a) diagrammatic drawing and (b) spot map

$$\frac{1}{R^*} = \frac{1}{R_1} + \frac{1}{R_2} \tag{3}$$

In a time-step, when the normal overlap α_n between adjacent ballast particles is larger than 0, the contact between the particles is identified. The normal contact force between particles F_n, the normal damping force F_η^d, the tangential contact force F_t, and the tangential damping force F_t^d can be calculated by Formula (4)–(10).

$$F_n = \frac{4}{3} E^* (R^*)^{1/2} \alpha_n^{3/2} \tag{4}$$

$$F_n^d = -2\sqrt{\frac{5}{6}}\beta\sqrt{S_n m^*} v_n^{rel} \tag{5}$$

$$F_t = -S_t \alpha_t \tag{6}$$

$$F_t^d = -2\sqrt{\frac{5}{6}}\beta\sqrt{S_t m^*} v_t^{rel} \tag{7}$$

$$\beta = \frac{-\ln e}{\sqrt{\ln^2 e + \pi^2}} \tag{8}$$

$$m^* = \frac{m_1 m_2}{m_1 + m_2} \tag{9}$$

$$\frac{1}{E^*} = \frac{1 - \mu_1^2}{E_1} + \frac{1 - \mu_2^2}{E_2} \tag{10}$$

where E^* and m^* are the equivalent elastic modulus and equivalent mass, R_1, R_2 are the radius of the two particles, μ_1, μ_2 are the Poisson's ratio of the two particles, E_1, E_2 are the elastic modulus of the two particles, e is the coefficient of restitution, S_n and S_t are the normal stiffness and tangential stiffness, α_t is a noninput parameter that represents the relative tangential displacement between two particles [25], as shown in Fig. 6. v_n^{rel} and v_t^{rel} are the normal and tangential components of relative velocity. The magnitude of the tangential force is limited by the Coulomb friction $\mu_s F_n$, where μ_s is the coefficient of friction. When the tangential force is less than the Coulomb friction, it is equal to the tangential force at the moment. When the tangential force is greater than the Coulomb friction, the particles slide at this moment, and the tangential force is equal to $\mu_s F_n$.

After obtaining the contact force and damping force at the contact between two ballast particles and between a ballast particle and geometric body, the velocities and displacements are,
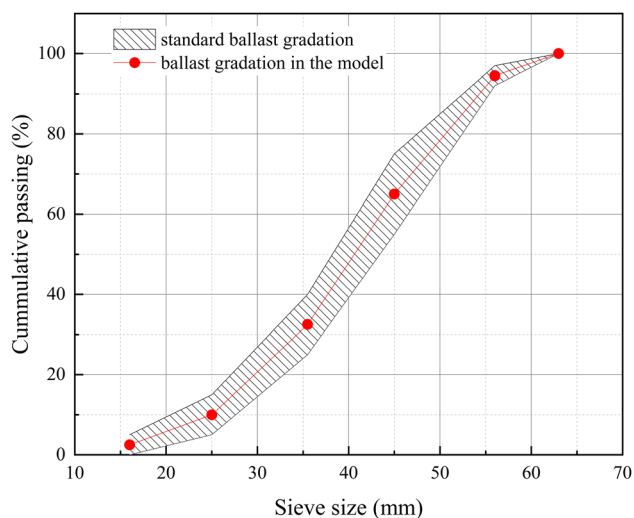

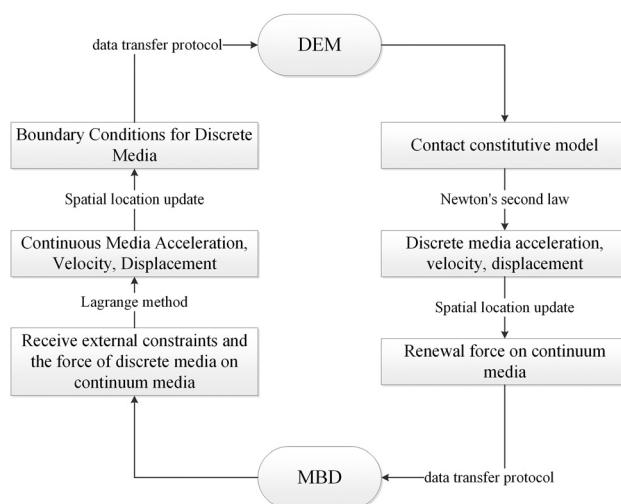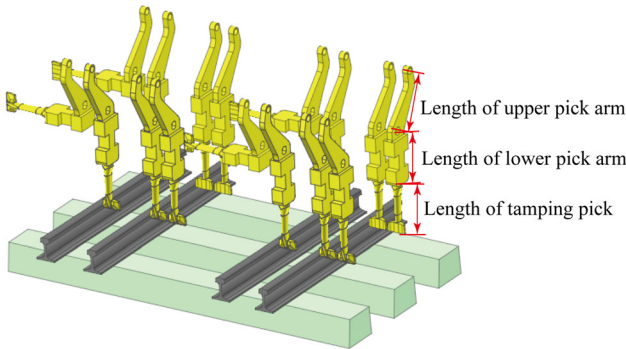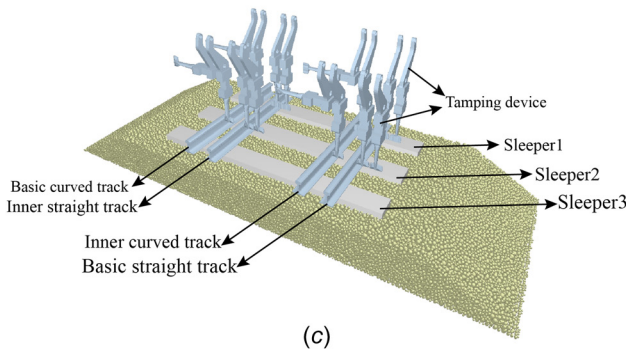**Fig. 2 Ballast gradation in the model**

Fig. 3 Coupled simulation flowchart of DEM and MBD

(a)

(b)

(c)

Fig. 4 DEM–MBD model of the turnout area: (a) CDC-16 turnout tamping device field measurement, (b) MBD model (RECURDYN), and (c) coupled model (EDEM–RECURDYN)

respectively, calculated in the DEM system and MBD system. After that, the spatial positions of particles and geometric bodies change. In the next time-step, the forces at contact positions are calculated again and another iteration begins. It is worth noting that in the data processing analysis, the direction in which the two particles approach each other is defined as the negative direction.
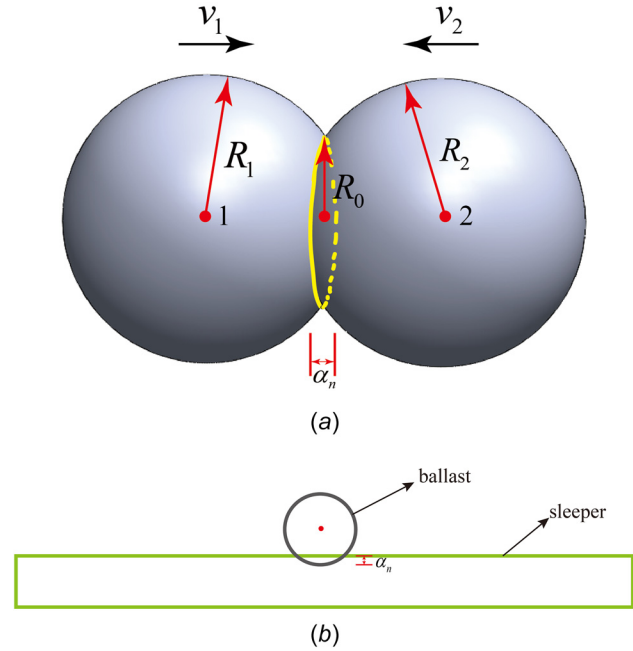

(a)

(b)

Fig. 5 Schematic diagram of the contact model: (a) contact between the ballast particles and (b) contact between the sleeper and the ballast

Therefore, it means that when the particles are approaching, the relative velocity is negative and vice versa.

2.3 Model validation. According to Refs. [26] and [27], the basic properties of the materials are formulated. Since the rail and ballast particles do not have direct contact, the contact parameters between the rail and ballast particles are not considered. References [28] and [29] are used to formulate the parameters of the rail, as shown in Table 2. Since the tamping device, sleepers, and ballast particles are in direct contact, in order to ensure the reliability of contact parameters, the calculation parameters of the simulation model are drawn up by referring to Refs. [18–20] and [30–32] and by means of control variable method, as shown in Table 3.

In fact, there is currently little research in this direction, and it is difficult to systematically conduct the field tests of tamping in railway turnout areas. Therefore, in order to verify the validity of the model, refer to the actual measurement results of the lateral resistance of the switch sleeper carried out in the turnout area in the literature [33].

In the simulation, the sleeper is pushed in the lateral direction at a constant speed of 1 mm/s and the lateral resistance and

Table 1 Dimensions of the model

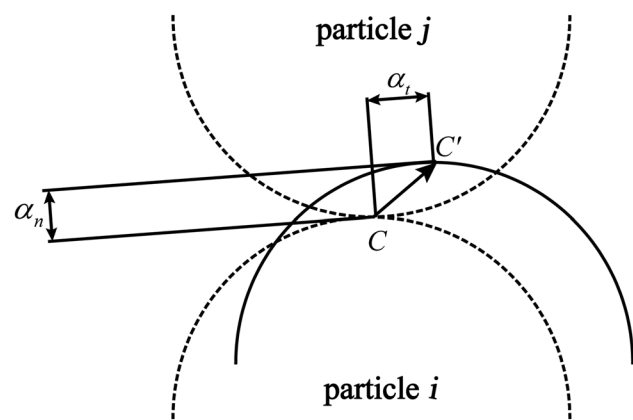| Component	Parameter	Value
Rail	type (kg·m^{-1})	60
Sleeper	Height (mm)	220
	Top width (mm)	260
	Bottom width (mm)	300
Ballast bed	Top surface width (mm)	3900
	Thickness (mm)	350
	Side slope grade	1:1.75
Tamping device	Length of upper pick arm (mm)	465
	Length of lower pick arm (mm)	359
	Length of tamping pick (mm)	495

Fig. 6 Schematic diagram of α_t and α_n at t moment

displacement of the sleeper are plotted, as shown in Fig. 7(a). Following Ref. [34], the work of lateral resistance can be calculated using Formula (11) and the lateral resistance work–displacement curve can be drawn in Fig. 7(b).

$$W = \int_{x_1}^{x_2} f(x)dx \tag{11}$$

where W is lateral resistance work, x is lateral displacement, and $f(x)$ is the lateral resistance at the x position.

According to Ref. [35], the lateral resistance at the displacement of 2 mm is used to access the track condition. As can be seen from Fig. 7(a), the lateral resistance in the simulation is 9.96 kN and that in the field test is 10.21 kN. The difference between them is 0.25 kN. Additionally, the lateral resistance work corresponding to 2 mm in the simulation and the field test in Fig. 7(b) is 14.86 kN mm and 16.10 kN mm, respectively, the difference of which is 1.24 kN mm. Therefore, the results of the simulation and the field test match well, indicating that the model can be used for further calculations.

3 Results Analysis

3.1 Microscopic contact Characteristics of Ballast Bed During Tamping Operation. According to the operational requirements of large tamping machines [18–20,26,32], the tamping operation in the turnout area can be divided into four stages, namely, the lifting stage (0–0.1 s), inserting stage (0.1–0.586 s), squeezing stage (0.586–1.186 s), and retracting stage (1.186–2.072 s).

In the lifting stage, the sleeper rises up at a speed of 0.3 m/s up to the height of 30 mm. In the inserting stage, the tamping device vibrates harmonically at a frequency of 35 Hz and an amplitude of 0.5 deg, while inserting the ballast bed structure downward at a speed of 1 m/s until the tamping depth (15 mm). In the squeezing stage, the tamping device rotates at the angular velocity of 10 deg per second and vibrates harmonically (the parameters are the same as the lifting stage). The purpose is to squeeze ballast particles between sleepers into the bottom. In the retracing stage, the tamping device releases at 15 deg per second and retracts at a speed of 1 m/s. Thus, a complete tamping operation cycle is achieved.

In order to explore the mechanical characteristics of the ballast bed in different stages of tamping operation, the effect of the tamping on the interaction between ballast particles is analyzed at the microscopic level. The distribution diagram of the force chain during tamping operation at the four stages is shown in Fig. 8.

As shown in Fig. 8, in the lifting stage, the sleeper is lifted upward and the disturbance to the ballast particles is small.

Table 2 Parameters used in the model

Component	Poisson ratio	Density (kg·m^{-3})	Shear modulus (GPa)
Ballast	0.18	2800	25
Sleeper	0.23	2300	15
Rail	0.30	7800	70
Tamping device	0.30	7800	70

Table 3 Contact parameters

Types	Coefficient of restitution	Coefficient of static friction	Coefficient of rolling friction
Ballast–ballast	0.50	0.80	0.05
Sleeper-ballast	0.50	0.70	0.10
Tamping deviceballast	0.50	0.40	0.10

Thus, the contact forces in the ballast bed are uniformly distributed. When entering the inserting stage, due to the vibration and insertion of tamping picks, the force chain of the ballast particles presents a downward transmission from the tip of tamping picks to the bottom of the ballast bed and the distribution is a cone at an angle roughly 45 deg. When entering the squeezing stage, with the clamping movement and the horizontal vibration of tamping picks, a concentrated distribution of the strong force chain appears under the sleeper. The distribution is approximately elliptical, with a depth of 150 mm. In the retracting stage, the upward movement and horizontal vibration of tamping picks cause a certain excitation on the nearby ballast particles, but the overall effect is slight. Additionally, the forces are significantly reduced, which shows that the ballast is in a loose status.

Coordination number is the number of contact points between each particle and its surrounding particles, which reflects the contact state of ballast particles. In order to further analyze the contact between ballast particles at various parts of the ballast bed during tamping operation, the ballast bed is divided into eight parts as shown in Fig. 9. The length and width of each part are
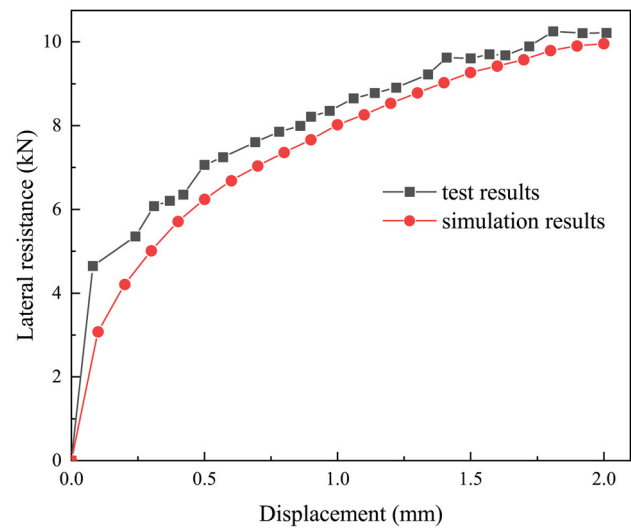
(a)
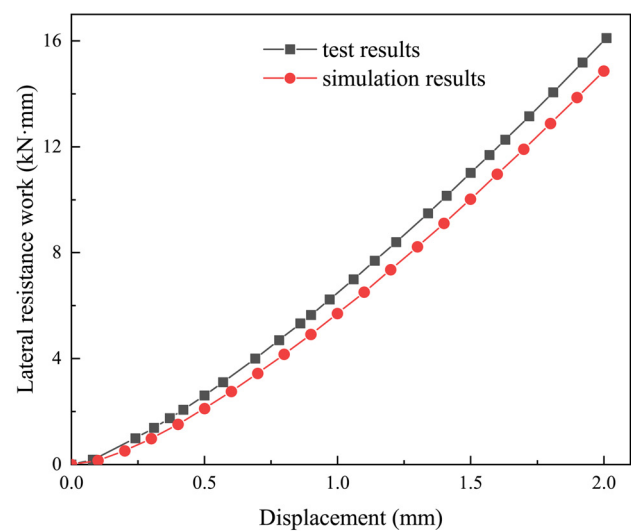
(b)

Fig. 7 Comparison between test and simulation: (a) lateral resistance–displacement curve and (b) lateral resistance work–displacement curve
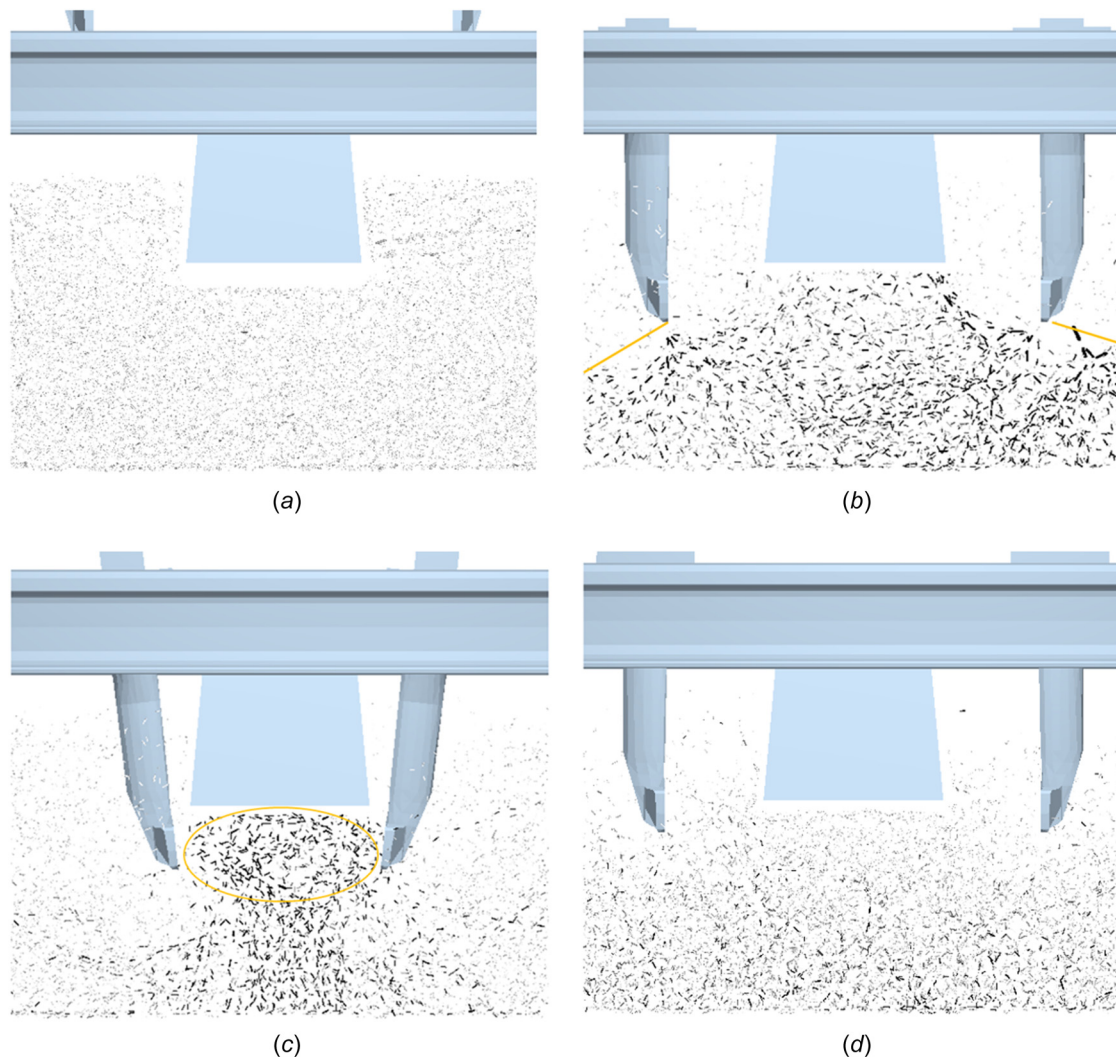
Fig. 8 Distribution diagram of the force chain during tamping operation: (a) lifting stage ($t = 0.1$ s, $F_{max} = 208.5$ N), (b) inserting stage ($t = 0.57$ s, $F_{max} = 4055.5$ N), (c) squeezing stage ($t = 1.18$ s, $F_{max} = 2784.4$ N), and (d) retracting stage ($t = 1.65$ s, $F_{max} = 407.4$ N)

2900 mm and 300 mm, respectively. The heights are different. J01 and J02 are in the sleeper crib, the height of which is 190 mm; J11 and J12 are in the lower part between sleepers, the heights of which are both 200 mm; J21 and J22 are under J11, J12, the heights of which are both 150 mm; D1, D2 are under the middle sleeper, the heights of which are 200 mm and 150 mm, respectively. The average contact force and coordination number of
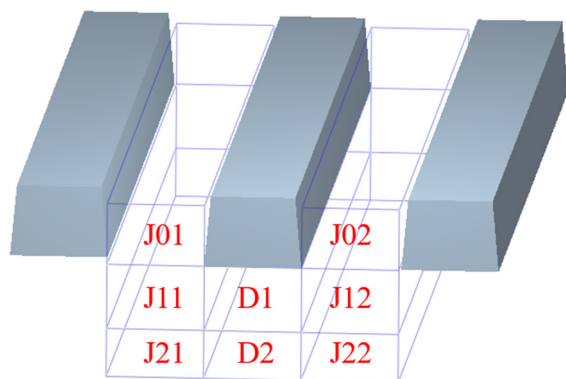

Fig. 9 Parts of the ballast bed

each part during tamping operation are collected and their time history curves are shown in Fig. 10.

As can be seen from Fig. 10, in the lifting stage, the contact force is small because the overall disturbance of the ballast bed is slight. However, at the moment of lifting sleepers, the stable state of the ballast bed is interrupted to a certain extent, leading to a small decrease in the coordination number. In the inserting stage, tamping picks are initially at the same level as the rail top and the buried depth of sleepers is 190 mm. Because tamping picks move downward to the ballast bed at 1 m/s, it takes about 0.2 s for tamping picks to encounter ballast particles. When the encounter occurs, the contact forces in the parts between sleepers (J01, J02, J11, J12, J21, J22) increase as the insertion depth grows. When tamping picks leave, the contact forces in the corresponding area decrease. In the squeezing stage, tamping picks have direct contact with the ballast particles in the D1 area. Thus, the maximum contact force in the D1 area appears in this period. Due to the clamping of tamping picks, the ballast particles in the D1 area are continuously compacted, so the contact force in the D1 area continues to increase. In the retracting stage, first, the tamping picks release from the squeezing final position to the vertical position, which lasts for 0.4 s, resulting in a certain extrusion on nearby ballast particles.

To sum up, the area of peak contact force varies with the position of the tamping pick during the tamping operation.

The inserting stage has the largest impact on the parts between sleepers, with the maximum contact force of about 680 N. The squeezing stage has the largest impact on the parts under sleepers, with the maximum contact force of about 1100 N.

3.2 Movement of Ballast Particles Under Tamping Operation. It is well known that the tamping operation of large machines destroys the equilibrium of the stress in the ballast bed. In order to further reveal the movement and distribution of ballast particles during the tamping operation, the nephograms of movement in the four stages are plotted, as shown in Fig. 11, wherein the arrow indicates the direction of particle movement and the color indicates the speed.

Figure 11 shows that there are great differences in the motion state of ballast particles at different stages. In the lifting stage, the rise of the sleeper interferes with the adjacent ballast particles. Thus, adjacent ballast particles show an upward movement trend with the sleeper, forming a diffusion angle of about 60 deg. However, the maximum speed in the stage is low, which is only 0.11 m/s. When entering the inserting stage, the exciting force and the insertion force of tamping picks have a significant impact on

the ballast in the sleeper crib, causing the ballast particles between sleepers to move down toward the bottom of the sleeper. The movement speed in this stage increases significantly and the maximum speed appears in the area near tamping picks. In the squeezing stage, tamping picks symmetrically turn at a certain angular velocity to squeeze the ballast particles to the bottom of the sleeper. The speeds of the ballast particles under the sleeper become much larger and the maximum speed appears around tamping picks. As a result, the loose part under the sleeper, formed in the lifting stage, is gradually filled and compacted. In the retracting stage, tamping picks retract with generating the harmonic vibration. The movement in this stage is exactly opposite to that in the inserting stage. The adjacent ballast particles move upward with tamping picks, while the ballast particles in other areas tend to be stable.

It can be seen from the above that the movement of ballast particles at various stages of tamping operation is very different. In order to better reflect the macroscopic state of ballast in different parts under tamping operation, the volume of ballast in different parts is collected and their compactness is calculated using the following equation:
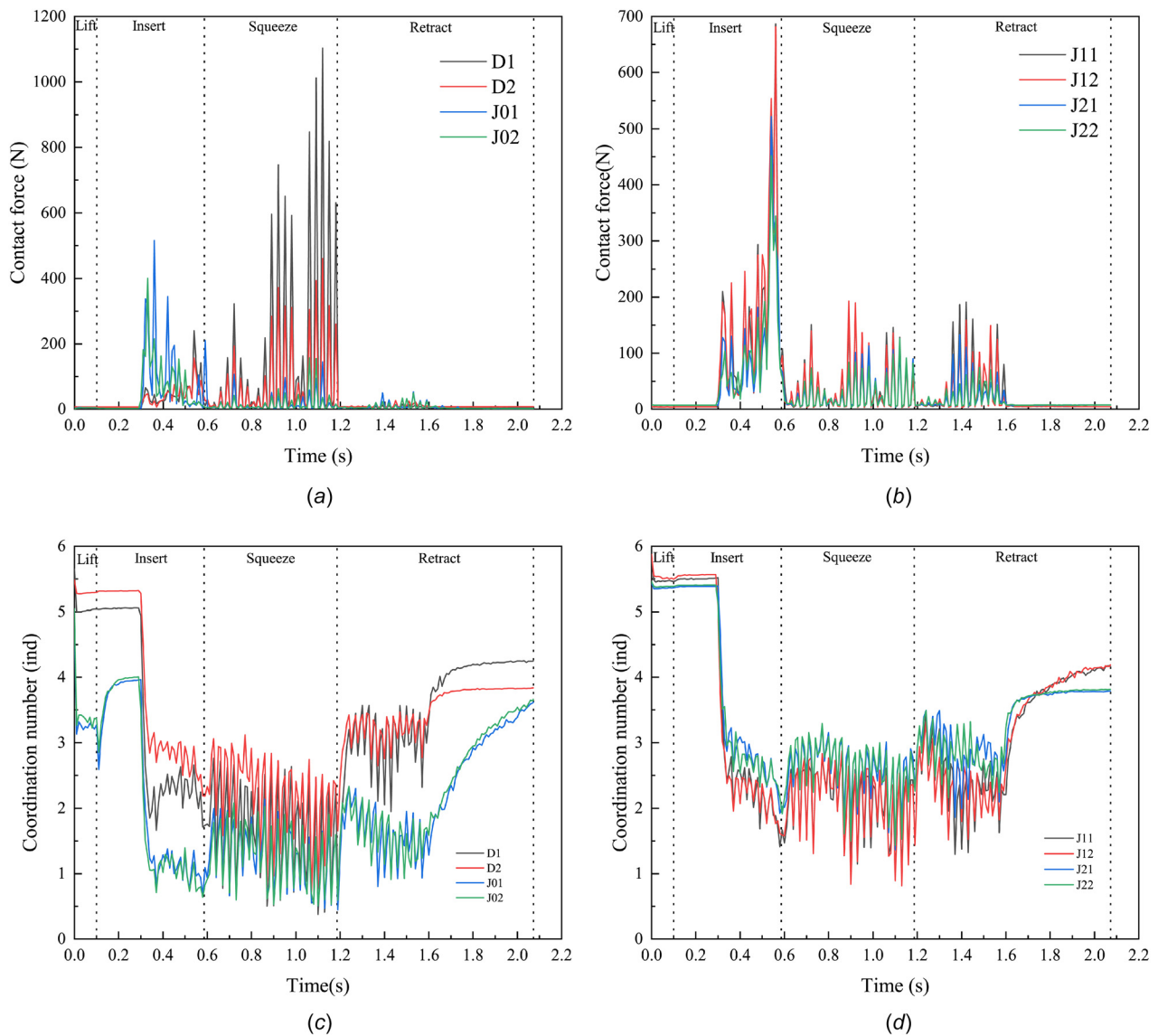

Fig. 10 Contact force and coordination number in the ballast bed during tamping operation: (*a*) contact force at D01, D02, J01, J02, (*b*) contact force at J11, J12, J21, J22, (*c*) coordination number at D01, D02, J11, J12, and (*d*) coordination number at J11, J12, J21, J22

$$D = \frac{V_S}{V} \qquad (12)$$

where V_S is the volume of the ballast in a part and V is the volume of the part. The compactness of the ballast in different parts during a tamping operation is shown in Fig. 12.

As seen from Fig. 12, the compactness in the sleeper crib (J01 and J02) decreases the most, by 27.4%, and that in the lower part between sleepers (J11, J12, J21, J22) decreases by 6.1%. In contrast, the compactness at the bottom of the sleeper (D1) increases by 5.9%. Additionally, the compactness also changes in different stages. The main purpose of tamping operation is to eliminate the void under sleepers and improve the compactness of the ballast under sleepers. Therefore, the following analysis focuses on the D1 area as an example. In the lifting stage, although the bottom of the sleeper appears void instantaneously after the lifting of the sleeper, the compactness in the D1 area does not vary much. In the inserting stage, due to the contact between tamping picks and ballast particles, the ballast in the sleeper crib moves downward, so that ballast particles are compacted and filled to the relatively loose area (D1) and consequently the compactness of the D1 area increases. In the squeezing stage, the compactness of the D1 area is further increased by clamping. In the meanwhile, the harmonic vibration generated by tamping picks causes the fluctuation of the compactness of the D1 area. In the retracting stage, the compactness of the D1 area tends to be stable.

In conclusion, the vibration and insertion of tamping picks cause the ballast bed to become loose. Regardless of the fact that the compactness of the D1 area at the bottom of the sleeper is improved, the uniformity of the ballast bed is reduced, which will reduce the longitudinal and lateral resistance of the ballast bed in the turnout area. Therefore, it is recommended that measures such as dynamic stability should be taken to improve the compactness of ballast between sleepers after tamping.

3.3 Study on the Influence of Tamping Operation Sequence. Because there are four rails, namely, two stock rails and two switching blades, the working condition of tamping in the turnout area is different from that in the main line. Because a tamping machine for turnouts has only four sets of tamping device and 16 tamping picks, it is impossible to complete the tamping of four rails at the same time. Usually, the tamping operation is performed in succession, for instance, first through track and then diverging track or vice versa. Here, the sequence can play a role in the tamping quality. In order to study the effect of sequence on tamping quality, two ways of tamping are simulated and changes in the compactness of the ballast under the sleeper (D1) are compared and discussed. The compactness of the ballast in D1 is compared in Fig. 13. The average contact force and coordination number of ballast particles in D1 are shown in Fig. 14.

It can be seen from Fig. 13 that when the sequence is first through and then diverging, the compactness in D1 is slightly higher than that of first diverging and then through, which accounts for 0.3%. Because the ballast particles under the sleeper are mainly affected in the squeezing stage as discussed in Sec. 3.1, the squeezing stage is selected for comparison. Figure 14 shows that the average contact force is relatively close when the sequence is first through and then diverging, meaning that the
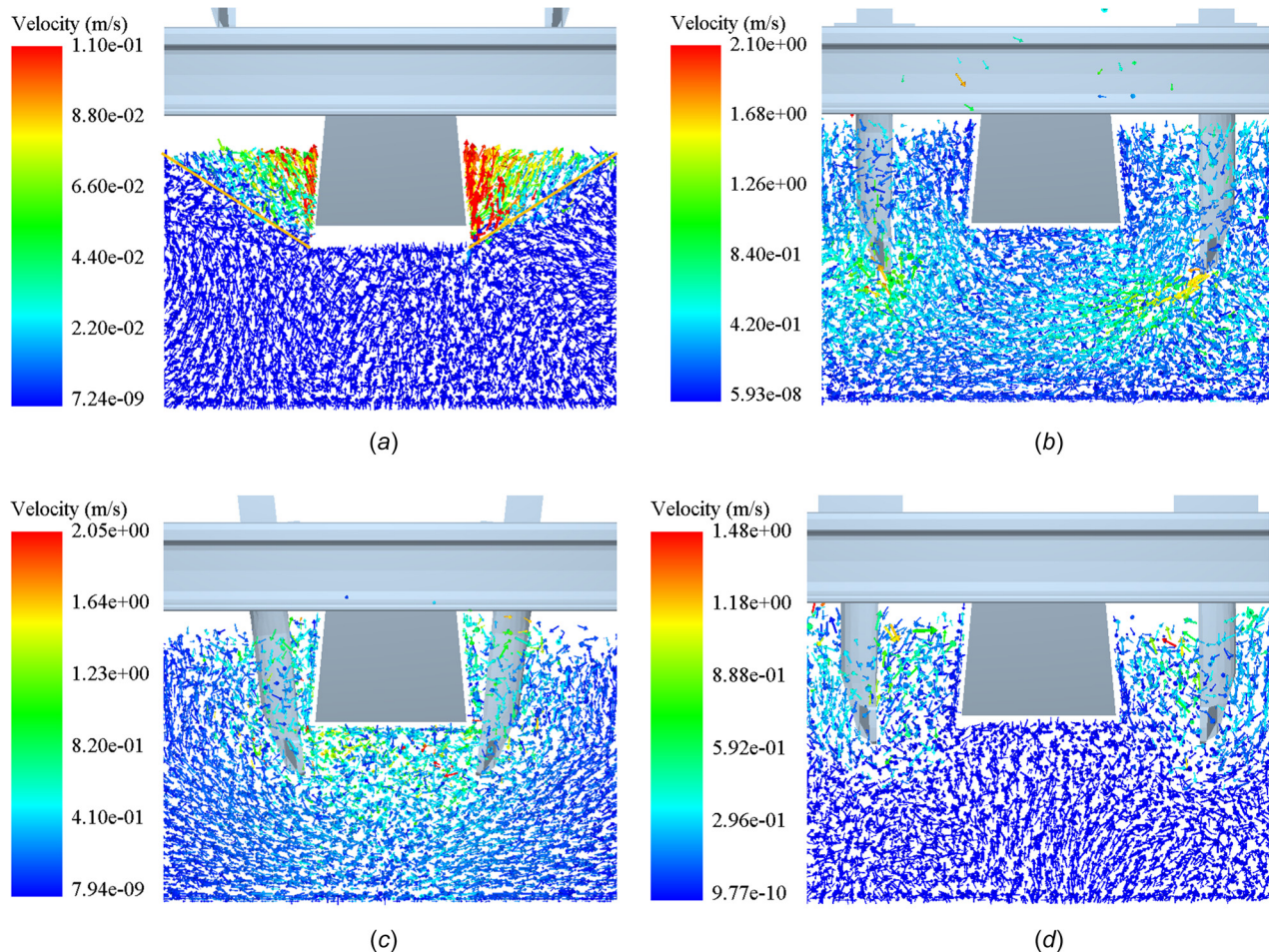

Fig. 11 Distribution of particle movement during tamping operation: (a) lifting stage ($t = 0.1$ s, $v_{max} = 0.11$ m/s), (b) inserting stage ($t = 0.57$ s, $v_{max} = 2.10$ m/s), (c) squeezing stage ($t = 1.18$ s, $v_{max} = 2.05$ m/s), and (d) retracting stage ($t = 1.65$ s, $v_{max} = 1.48$ m/s)
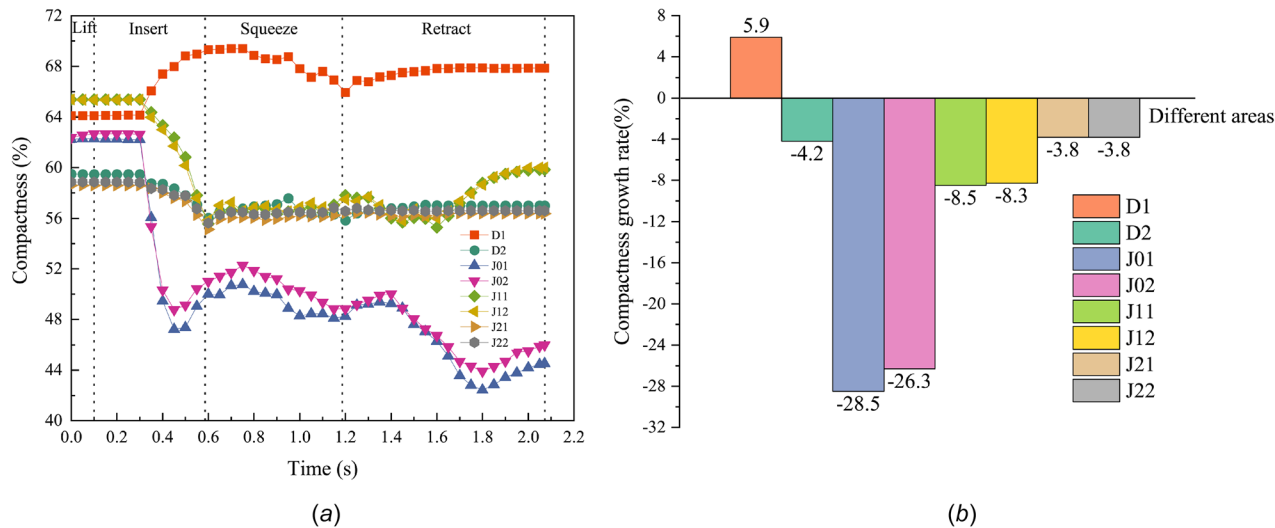
Fig. 12   Variation of compactness in different areas during tamping operation: (*a*) compactness in different parts and (*b*) changes in compactness in different parts
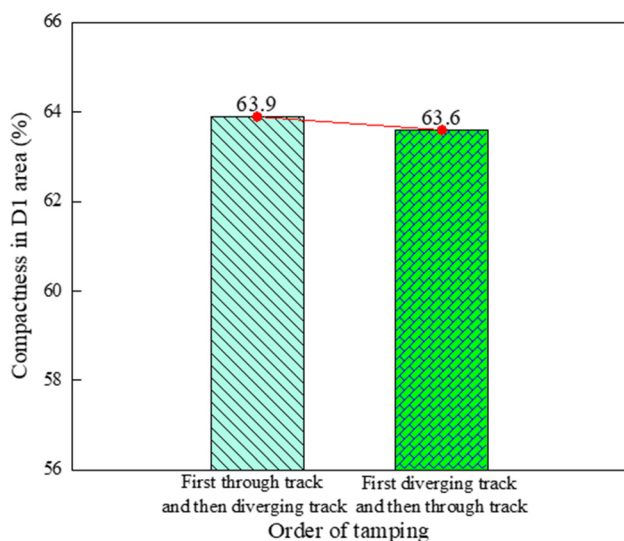

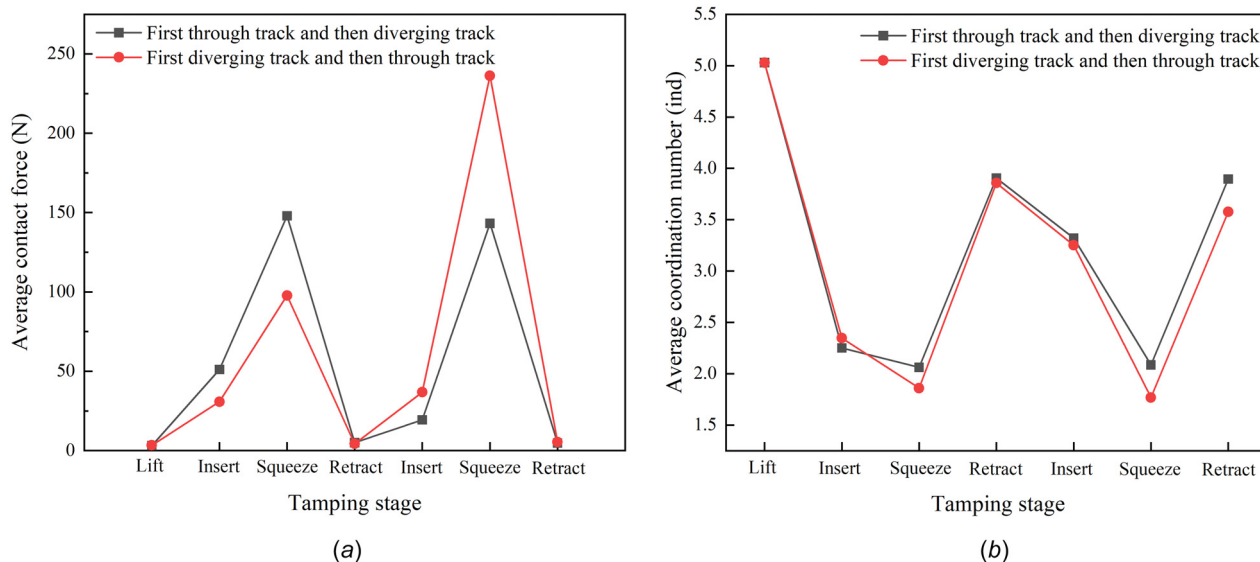**Fig. 13   Compactness in D1 with different tamping sequences**

number of the particles pushed in different areas is similar in two tamping operations and consequently the uniformity of the ballast bed is better. Additionally, the average coordination number in this sequence is large, indicating that the contact state of ballast particles is better. To sum up, it is recommended to use the sequence of first through track and then diverging track for the tamping operation at the switching part of turnout areas.

4   Conclusions

(1) In the paper, a dynamic model considering a large tamping device, rail, sleeper, and ballast bed at the switching part of turnout areas has been developed using the EDEM–RECURDYN coupling method and validated. Through the coupling algorithm of two software, the complex tamping operation is accurately simulated and the interactions between tamping picks, sleepers and ballast particles are analyzed.

(2) During the tamping operation at the switching part in turnout areas, strong force chains concentrately distribute under lifted sleepers due to the clamping and the horizontal vibration of tamping picks. The distribution range is approximately elliptical, with a depth of about 150 mm.

Fig. 14   Contact status in ballasts with different tamping sequences: (*a*) average contact force and (*b*) average coordination number

The maximum contact force in the ballast between sleepers appears in the late inserting stage, about 680 N, while the maximum contact force in the ballast under the sleeper appears in the late squeezing stage, about 1100 N.

(3) With the inserting of tamping picks, ballast particles in the sleeper crib move downward. After that, ballast particles between sleepers move to the bottom of the sleeper due to the clamping movement of tamping picks. After tamping, the compactness of the ballast in the sleeper crib decreased by 27.4% and that in the lower part between sleepers decreased by 6.1%. In contrast, the compactness at the bottom of the sleeper increases by 5.9%. It is recommended that measures such as dynamic stability should be taken to improve the compactness of ballast between sleepers after tamping.

(4) By changing the sequence of the tamping operation, the compactness of the ballast under the sleeper is similar, but the contact status of ballast particles are different. It is recommended to use the sequence of first through track and then diverging track for the tamping operation at the switching part of turnout areas.

Funding Data

References

[1] Ergenzinger, C., Robert Seifried, J., and Eberhard, A. P., 2012, "A Discrete Element Approach to Model Breakable Railway Ballast," ASME J. Comput. Nonlinear Dyn., 7(4), p. 041010.

[2] Feng, B., Basarah, Y. I., Gu, Q., Duan, X., Bian, X., Tutumluer, E., Hashash, Y. M., and Huang, H., 2021, "Advanced Full-Scale Laboratory Dynamic Load Testing of a Ballasted High-Speed Railway Track," Transp. Geotech., 29(6), p. 100559.

[3] Lackenby, J., Indraratna, B., Mcdowell, G., and Christie, D., 2007, "Effect of Confining Pressure on Ballast Degradation and Deformation Under Cyclic Triaxial Loading," Géotechnique, 57(6), pp. 527–536.

[4] Hiroyuki, S., Yoshimitsu, T., and Ryosuke, M., 2011, "Analysis of Wheel/Rail Contact Geometry on Railroad Turnout Using Longitudinal Interpolation of Rail Profiles," ASME J. Comput. Nonlinear Dyn., 6(2), 024501.

[5] Kampczyk, A., and Dybe, K., 2021, "The Fundamental Approach of the Digital Twin Application in Railway Turnouts With Innovative Monitoring of Weather Conditions," Sensors, 21(17), p. 5757.

[6] Guo, Y., Markine, V., and Jing, G., 2021, "Review of Ballast Track Tamping: Mechanism, Challenges and Solutions," Constr. Build. Mater., 300, p. 123940.

[7] Przybyłowicz, M., Sysyn, M., Gerber, U., Kovalchuk, V., and Fischer, S., 2022, "Comparison of the Effects and Efficiency of Vertical and Side Tamping Methods for Ballasted Railway Tracks," Constr. Build. Mater., 314, p. 125708.

[8] Kumara, J. J., and Hayano, K., 2016, "Deformation Characteristics of Fresh and Fouled Ballasts Subjected to Tamping Maintenance," Soils Found., 56(4), pp. 652–663.

[9] Mcdowell, G. R., Lim, W. L., Collop, A. C., Armitage, R., and Thom, N. H., 2005, "Laboratory Simulation of Train Loading and Tamping on Ballast," Proc. Inst. Civ. Eng. Transp., 158(2), pp. 89–95.

[10] Douglas-S C, 2013, "Railroad Ballast Quality and Break Down During Tamping," Douglas-S C, Indianapolis, IN.

[11] Aingaran, S., Pen, L. L., Zervos, A., and Powrie, W., 2018, "Modelling the Effects of Trafficking and Tamping on Scaled Railway Ballast in Triaxial Tests," Transp. Geotech., 15, pp. 84–90.

[12] Wang, W., Song, S., Yan, H., Xiao, B., and Zeng, Z., 2018, "Experimental Study on Resistance Characteristics of Ballast Bed in Different Stamping Stages," J. Cent. South Univ. (Sci. Technol.), 49(8), pp. 2003–2008.

[13] Tutumluer, E., Huang, H., and Hashash, Y., 2006, "Aggregate Shape Effects on Ballast Tamping and Railroad Track Lateral Stability," AREMA 2006 Annual Conference, Louisville, KY, Sept. 17–20.

[14] Saussine, G., Azéma, E., Gautier, P. E., Peyroux, R., and Radjaï, F., 2012, "Numerical Modeling of the Tamping Operation by Discrete Element Approach," World Congress on Rail Research, South Korea, pp. 1–9.

[15] Saussine, G., Azéma, E., Perales, R., Radjaï, F., Nakagawa, M., and Luding, S., 2009, "Compaction of Railway Ballast During Tamping Process: A Parametric Study," Am. Inst. Phys., 1145(1), pp. 469–472.

[16] Wang, X. J., Chi, Y. L., Li, W., Zhou, T. Y., and Geng, X. L., 2012, "The Research of the Numerical Simulation on the Granular Ballast Bed Tamping," Adv. Mater. Res., 479–481, pp. 1395–1398.

[17] Wang, X. J., Chi, Y. L., Li, W., and Zhou, T. Y., 2012, "Study on the DEM Simulation of the Granular Railway Ballast Bed Tamping," Adv. Mater. Res., 524–527, pp. 3256–3259.

[18] Shi, S., Gao, L., Cai, X., Yin, H., and Wang, X., 2020, "Effect of Tamping Operation on Mechanical Qualities of Ballast Bed Based on DEM-MBD Coupling Method," Comput. Geotech., 124, p. 103574.

[19] Shi, S., Gao, L., Xiao, H., Xu, Y., and Yin, H., 2021, "Research on Ballast Breakage Under Tamping Operation Based on DEM–MBD Coupling Approach," Constr. Build. Mater., 272, p. 121810.

[20] Zhou, T., Hu, B., and Sun, J., 2013, "Study of Railway Ballast Compactness Under Tamping Operation," J. Appl. Sci., 13(11), pp. 2072–2076.

[21] Feng, B., 2014, Design and Simulation Study of Tamping Mechanism Test Device, Southwest Jiaotong University, Chengdu, China.

[22] Jing, G., Siahkouhi, M., Qian, K., and Wang, S., 2021, "Development of a Field Condition Monitoring System in High Speed Railway Turnout," Measurements, 169, p. 108358.

[23] Zhang, Z., Xiao, H., Wang, M., Liu, G., and Wang, H., 2021, "Mechanical Behavior and Deformation Mechanism of Ballast Bed With Various Fouling Materials," J. Central South Univ., 28, pp. 2857–2874.

[24] Ngo, N. T., Indraratna, B., and Rujikiatkamjorn, C., 2014, "DEM Simulation of the Behaviour of Geogrid Stabilised Ballast Fouled With Coal," Comput. Geotechnics, 55, pp. 224–231.

[25] Mindlin, R. D., and Deresiewicz, H., 1953, "Elastic Spheres in Contact Under Varying Oblique Forces," J. Appl. Mech., 20(3), pp. 327–344.

[26] Liu, J., Wang, P., Liu, G., Xiao, J., Liu, H., and Gao, T., 2020, "Influence of a Tamping Operation on the Vibrational Characteristics and Resistance-Evolution Law of a Ballast Bed," Constr. Build. Mater., 239, p. 117879.

[27] Feng, B., Park, E. H., Huang, H., Li, W., Tutumluer, E., Hashash, Y. M., and Bian, X., 2019, "Discrete Element Modeling of Full-Scale Ballasted Track Dynamic Responses From an Innovative High-Speed Rail Testing Facility," Transp. Res. Rec., 2673(9), pp. 107–116.

[28] Zhai, W., Wang, K., and Cai, C., 2009, "Fundamentals of Vehicle-Track Coupled Dynamics," Veh. Syst. Dyn., 47(11), pp. 1349–1376.

[29] Zhai, W., and Wang, K., 2010, "Lateral Hunting Stability of Railway Vehicles Running on Elastic Track Structures," ASME J. Comput. Nonlinear Dyn., 5(4), pp. 2040–2049.

[30] Yahia, A., and Mohammed, H., 2021, "Geomechanical Modelling of Railroad Ballast: A Review," Arch. Comput. Methods Eng., 28(3), pp. 815–839.

[31] Wang, L., Zhao, Z., Wang, J., Li, X., Huang, Y., and Yao, T., 2021, "Mechanical Characteristics of Ballast Bed Under Dynamic Stabilization Operation Based on Discrete Element and Experimental Approaches," Shock Vib., 2021, p. 6627612.

[32] Shi, S., Gao, L., Cai, X., Xiao, Y., and Xu, M., 2022, "Mechanical Characteristics of Ballasted Track Under Different Tamping Depths in Railway Maintenance," Transp. Geotech., 35, p. 100799.

[33] Yan, H., 2017, "Experimental Study on Resistance of Ballast Bed Under Different Length Turnout Sleepers," J. Railw. Sci. Eng., 14(06), pp. 1225–1230.

[34] Liu, J., Chen, R., Liu, Z., Liu, G., Wang, P., and Wei, X., 2021, "Comparative Analysis of Resistance Characteristics of Composite Sleeper and Concrete Sleeper in Ballast Bed," Constr. Build. Mater., 300(2), p. 124017.

[35] Mansouri, P., Zakeri, J. A., and Mohammadzadeh, S., 2021, "Numerical and Laboratory Investigation on Lateral Resistance of Ballasted Track With HA110 Sleeper," Constr. Build. Mater., 301(4), p. 124133.